GEOPHYSICAL RESEARCH LETTERS, VOL. 37, L03605, doi:10.1029/2009GL041890, 2010

A deep-ocean Kelvin-Helmholtz billow train

Hans van Haren[1] and Louis Gostiaux[2]

Received 23 November 2009; revised 7 January 2010; accepted 14 January 2010; published 6 February 2010.

[1] Detailed overturning is observed between 0.5 and 50 m above the sloping side of Great Meteor Seamount, Canary Basin, using 100 moored temperature sensors, 1 mK accurate, sampling at 1-Hz. While previously reported frontal bores of 40-m amplitude can form with vigorous near-bottom motions and sediment resuspension at the beginning of the upslope phase of large, e.g., tidal, carrier waves, the downslope phase presented here is more "permanently" turbulent away from the bottom. This turbulence is inferred from high-resolution temperature space-time series, which reveal ubiquitous "finger-like" structures. It occurs during the clear-water tidal phase, with low amounts of acoustic scatterers. The high-frequency finger-like motions $\sigma \gg$ N, N the buoyancy frequency, are observed simultaneously with local mode-2 near-N inertio-gravity waves and overall shear $|S| \approx N$. They show large temperature variations, 5–10 m vertical amplitudes and occasionally develop Kelvin-Helmholtz billows. The typical (Eulerian) period of these firstly observed deep-ocean billows amounts 50 ± 10 s. **Citation:** van Haren, H., and L. Gostiaux (2010), A deep-ocean Kelvin-Helmholtz billow train, *Geophys. Res. Lett.*, *37*, L03605, doi:10.1029/2009GL041890.

1. Introduction

[2] In the search for the dominant processes of mixing in the ocean, sloping bottom boundaries still constitute an important site. There, internal waves may focus their energy, become non-linear and eventually break. Whether or not important for ocean mixing as a whole, as addressed by, e.g., *Garrett* [1990], vigorous motions do occur above sloping sea floors as recently revealed via precise, fast-sampling observations. However, detailed observations from the deep ocean linking internal waves and turbulent mixing are scarce.

[3] As processes driving turbulent motions may have different scales, it is necessary to distinguish the different time scales observed in bottom boundary layers. These scales range from those associated with large-scale flows, those associated with energetic internal waves like tides and those associated with strongly non-linear bore-like motions. Frontal bores can produce large transport of resuspended materials up a sloping bottom [*Klymak and Moum*, 2003; *Hosegood et al.*, 2004]. They have a Eulerian time scale O(10^2)s, but are generated by process such as tidal and atmospheric forcing that have time scales O(10^5)s. This upslope turbulent transport contrasts with the common assumptions about sloping bottom boundary layers, which predict asymmetric growth of these layers and ditto turbulent mixing with largest values during a downslope favourable flow [*Weatherly and Martin*, 1978; *MacCready and Rhines*, 1993]. Typical timescale for set-up and growth of such downslope flow boundary layer is O(10^5–10^6)s.

[4] Vigorous short-term, $<10^3$s, current variations have indeed been observed ubiquitously occurring at some distance O(10 m) from the bottom above a sloping side of the Faeroe-Shetland Channel, uniquely during the downwelling favourable phase of the dominant alongslope flow [*Hosegood and van Haren*, 2003]. The periodicity of the boundary flow was about 4 days and most likely atmospherically forced. At the time, the instrumental set-up using mechanical current meters sampling at a rate of once per 30 or 60 s did not allow determination of the turbulence processes. This could be free convection as the downslope favourable flow is thought to create barely stable and large, homogeneous bottom boundaries.

[5] Here we demonstrate that in, shorter periodic, tidally dominated flows the downslope phase is dominated by another turbulence process: the stratification is not weak per se and supports Kelvin-Helmholtz (K-H) type overturning billows that are created by large-scale internal wave shear. A mechanism for internal wave-induced mixing is 'shear instability', whereby 'large-scale' motions, more commonly low-frequency internal waves near the inertial frequency f, create vertical shear upon which small-scale high-frequency internal waves at or just below the buoyancy frequency N become deformed and eventually break [e.g., *Phillips*, 1977].

[6] Such K-H instabilities are well-observed in the laboratory [e.g., *Thorpe*, 1971], but also in the atmosphere where they are also known as "clear-air turbulence", occurring at unsaturated altitudes with few clouds [*Ludlam*, 1967; *Browning and Watkins*, 1970]. In the ocean, near-surface observations have been made using dye [*Woods*, 1968], temperature sensors [e.g., *Marmorino*, 1987] and acoustics [e.g., *Haury et al.*, 1979; *Moum et al.*, 2003]. Some of these observations [*Marmorino*, 1987] confirmed theoretical suggestions [*Hazel*, 1972] that fully turbulent K-H billows occur where the gradient Richardson number $Ri = N^2/|\mathbf{S}|^2 < 0.25$, the criterion for linear (in)stability [*Miles*, 1961; *Howard*, 1961]. Here, $\mathbf{S} = [\partial u/\partial z, \partial v/\partial z]$ denotes the shear vector for horizontal current components u and v. In contrast, *Grue et al.* [2000], in the laboratory, and *Moum et al.* [2003], near the surface in the ocean, observed beautiful and rare K-H rollup associated with near-surface internal solitary waves whilst Ri > 1. This could be explained from the more relaxed instability criterion for 3D flows [*Abarbanel et al.*, 1984], but may also be due to the poor shear length-scale resolution, as suggested by *Moum et al.* [2003]. Ri ≈ 0.1 have been observed in thin interfaces of breaking soli-

[1]Royal Netherlands Institute for Sea Research, Den Burg, the Netherlands.
[2]Coriolis, LEGI, CNRS, Grenoble, France.

0094-8276/10/2009GL041890$05.00

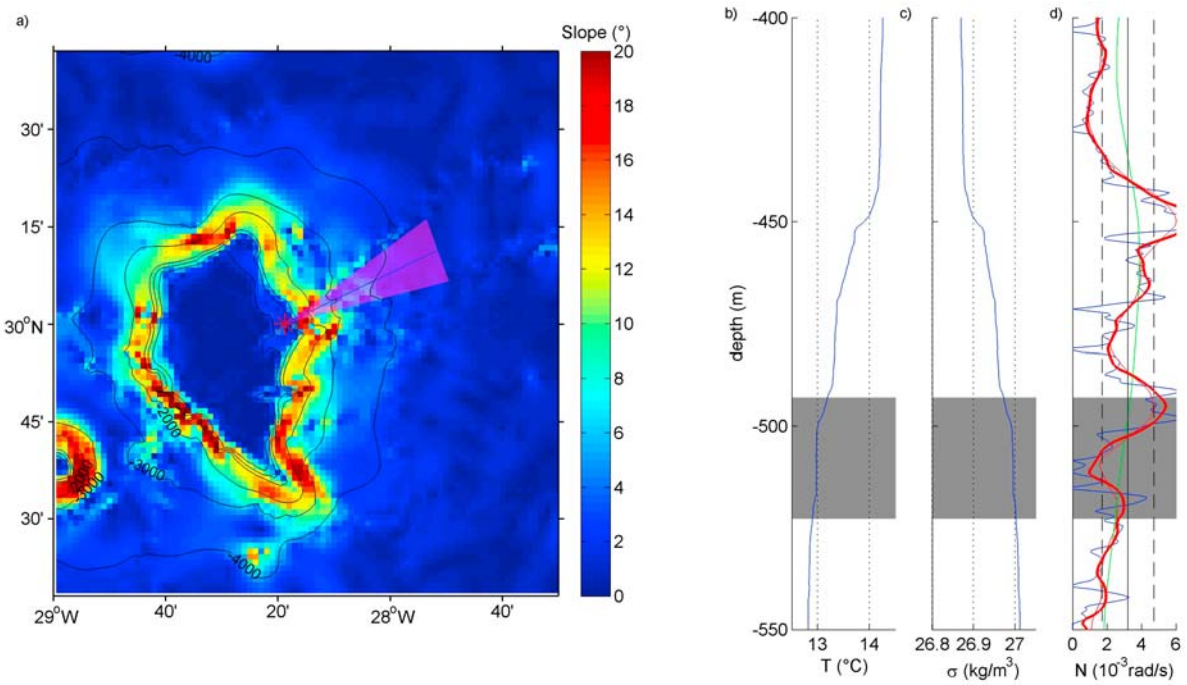

Figure 1. (a) Location of mooring and CTD-station (red star) on contours of bathymetry and color map of bottom-slopes, computed from 1′-topography [*Smith and Sandwell*, 1997]. Purple arrow indicates direction of internal waves. Unlabeled contour-lines correspond to z = −400 m, −600 m and −800 m. (b) Temperature from CTD. (c) Potential density. (d) N-profiles computed for Δz = 100 m (green), 10 m (red) and 1 m (blue); vertical lines correspond to $N = 3.2 \pm 1.5 \times 10^{-3}$ s^{-1}. In Figures 1b–1d the shadowed region corresponds to temperature range [12.9 13.2]°C where K-H instabilities develop.

tary waves in the laboratory [*Fructus et al.*, 2009]. The fastest growing instabilities have an estimated wavelength of $\lambda = 7.5\Delta z$, where Δz denotes the thickness of the shear layer. K-H billows are thus expected in crests and troughs of an internal wave where shear is largest. No detailed observations of them exist from the deep-ocean, or related to (sloping) bottom layers. Such observations will be presented in this paper.

2. Data and Background

[7] We taped 96 custom-made "NIOZ3" temperature sensors to a nylon-coated steel mooring cable at 0.5 m intervals. This "thermistor string" was mounted 2 m above the bottom to an aluminium bottom lander frame. The frame held 3 additional sensors, so that the lowest sensor was nominally at 0.5 m from the bottom. The frame also held a 300 kHz Teledyne RDI acoustic Doppler current profiler ADCP and a Nortek AquaDopp acoustic current meter. Another AquaDopp was 10 m below the elliptical top-buoy of the 160-m long mooring line. The lander was moored at 30° 00.052′N, 28° 18.802′W, H = 549 m water depth, near the top of the eastern slope of Great Meteor Seamount (GMS) for 18 days in May/June 2006. The bottom slope was 4 ± 1° and globally orientated ENE as estimated from bathymetry and echosounder data (Figure 1).

[8] The NIOZ3 thermistors sampled at 1 Hz with accuracy better than 0.001°C [*van Haren et al.*, 2009]. The current meters sampled at 0.2 Hz and the ADCP at 0.5 Hz. Unfortunately, the ADCP-data are rather noisy due to regular lack of scatterers in combination with occasional hard reflectance at thermistors.

[9] A few shipborne CTD-profiles demonstrated that the local stratification is $N = 3.2 \pm 1.5 \times 10^{-3}$ s^{-1} where a vertical length scale of 10 m is used in the computation. This results in an average semidiurnal internal tide slope of 1.5°, so that the local bottom slope is significantly different from critical. In the area, density variations are dominated by temperature T variations over salinity S variations, by an absolute factor of 1.5–2 with S decreasing with depth like T, so that the moored T-data are an adequate tracer for density variations.

[10] GMS is known for its variation in tidal motions, with a dominance of semidiurnal tidal motions near its northern tip, the present mooring site, and a dominance of diurnal motions above its southern flanks [*Mohn and Beckmann*, 2002]. In general, the diurnal frequency coincides with f at which, in particular at these latitudes, large-scale O(10 m) vertical shear is dominant, at least in the open ocean [*van Haren*, 2007].

3. Observations

[11] The semidiurnal tidally dominated near-bottom T-variations show the familiar fortnightly spring-neap cycle, besides a weak diurnal inequality (Figure 2). In the overall pattern none of the tidal variations is sinusoidal in shape, but more cnoidal, and asymmetric as well. These slow T-increases followed by a sudden drop are associated with the down- and up-slope phases of the tidal currents. The eccentricity of the lunar M_2 tidal ellipse is 1.7 and its main axis of heading 67° ± 10 is orientated along the slope. The sudden frontal T-drops pass the sensors within a few minutes. They are associated with a brief strictly upslope

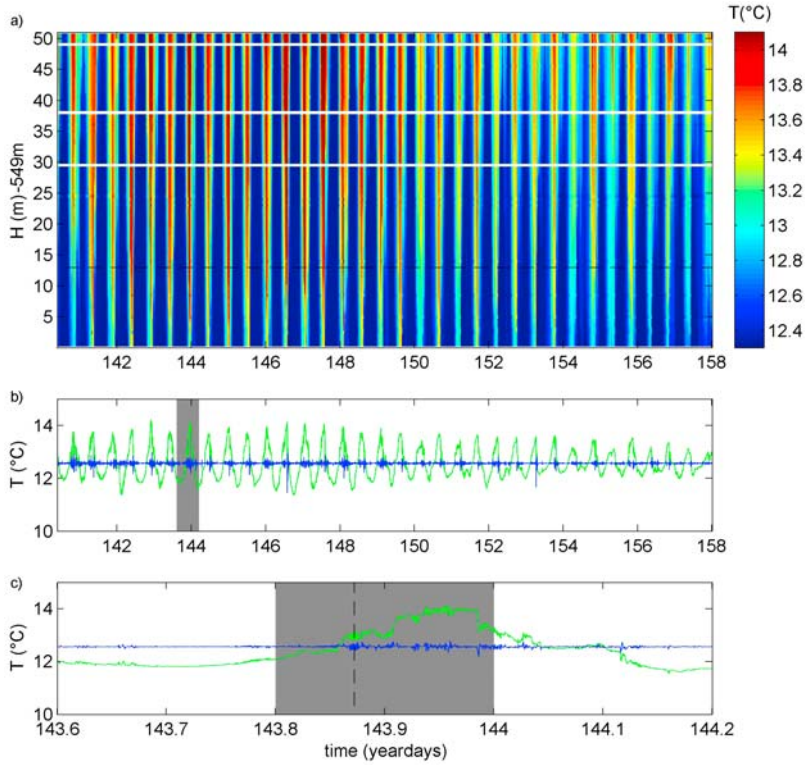

Figure 2. (a) Total depth-time series of temperature data measured by 100 sensors at 1 Hz between 0.5 and 50 m above the bottom near the top of Great Meteor Seamount. White lines indicate missing sensors. (b) Entire temperature record (green) and associated high-frequency part (blue filter window 0.01–0.2 Hz) from the sensor located 13 m above the bottom, corresponding to the dashed line in Figure 2a. The shadowed region corresponds to Figure 2c. (c) About half-day detail of Figure 2b. The shadowed region corresponds to Figure 3a time interval and the vertical dashed line to yearday 143.872, when strongest K-H instabilities occur.

flow when most vigorous and with strong vertical currents and sediment resuspension [*Hosegood et al.*, 2004]. These backwards breaking waves show amplitudes up to 45 m above the bottom. During none of the tidal cycles they occur at precisely the same moment or in the same shape [*van Haren*, 2006].

[12] Here, we do not focus on T-variations associated with the front that create spikes in high-frequency T-signals (blue graph in Figure 2b), but on moderate T-bursts over longer periods during the downslope phase of the tide. Such moderately vigorous T-variations are nearly omnipresent during this longer duration tidal phase (Figure 2c). It is noted that the time series from a single depth is somewhat misleading, because the vigorous T-variations are associated with the largest stratification, the "pycnocline", that caps the less stratified bottom boundary layer. As the latter can reach up to 50 m above the bottom while seldom becoming homogeneous in a stratification sense, and as the pycnocline above it is typically 10 m thick, the passage of associated turbulent motions at a particular depth varies with time (Figure 3).

[13] The downslope phase of the semidiurnal tidal internal wave becomes superposed with smaller scale high-frequency waves that have periods of up to 15 minutes (Figure 3a). Such periods are just about larger than the buoyancy period computed over thin interfaces O(1 m) and may thus constitute free internal waves. As with the upslope phase, none of the downslope tidal phases shows precisely the same

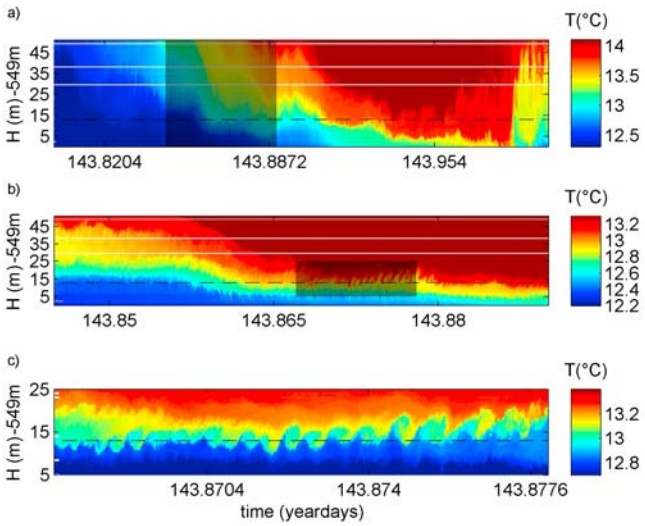

Figure 3. (a and b) Example of temperature variations during a downslope tidal phase at different time scales; the shadowed regions in Figures 3a and 3b highlight the (c) time range. Only in Figure 3c all data points are included from the 1-Hz sampled thermistors. In all plots white lines indicate missing sensors. The dashed line shows the sensor from which time series in Figures 2b and 2c are extracted. Note the color scales change and the different vertical range in Figure 3c.

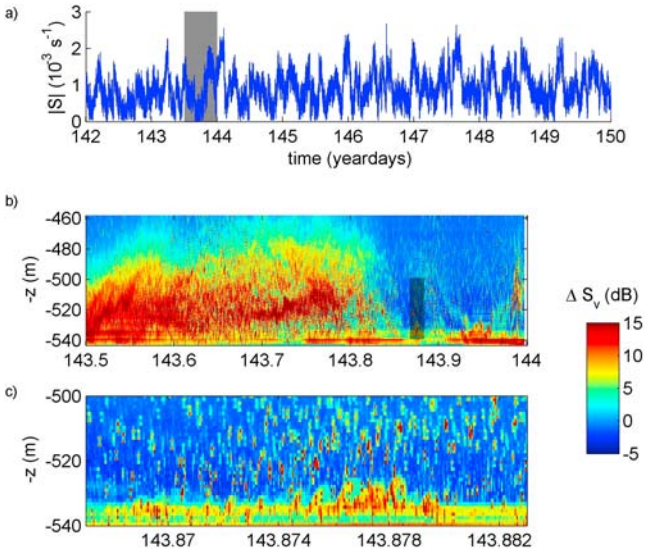

Figure 4. (a) Shear computed between the two current meters at 1.5 and 151.5 m above the bottom. (b) Zoom of ADCP's relative backscattering strength data with time for one tidal period. (c) Further zoom corresponding to the shadowed region in Figure 4b.

pattern in high-frequency waves. These waves are quasi-randomly distributed. Likewise, they change appearance with time, from familiar vertical mode-1 to mode-2 across a typical range of pycnocline thickness O(10 m). This may indicate preceding wave-breaking [*Sveen et al.*, 2002].

[14] Superposed on the high-frequency internal waves are found higher-frequency variations, which cannot be free internal waves. They are slanted or curved, due to the sheared current associated with the waves and background, low-frequency [internal wave] flow, they have a vertical extent O(10 m) and they appear as 'fingers' intruding in the weaker stratified fluid below (Figures 3a and 3b). They resemble intrusions often observed in atmospheric clouds. They are not uniquely associated with a particular phase of small-scale internal waves.

[15] Zooming in further detail they appear as K-H overturns or billows, although seldom as beautiful as in (Figure 3c). The separation in time between the fingers or billows is 50 ± 10 s and some 10 are formed in a train. The typical wavelength is estimated at $\lambda = 75$ m, using the 10-m vertical shear-scale. Like with the upslope moving frontal bores, these smaller-scale billows each have different form or stage of development. Some appear as cusps, others are a near-perfect role-up, or show a blurred turbulent wake in their core.

[16] The associated large-scale shear is $|\mathbf{S}| = 2.2 \pm 0.2 \times 10^{-3}$ s^{-1} computed between current meters over 150 m (Figure 4), with a dominant tidal periodicity. This weakly dominant tidal current difference variance is less than 4 times the inertial variance, while the current variance ratio of tides over inertial motions amounts 20. At the same latitude but in the open ocean, 10-m shear is far dominant over tidal shear, by a factor of 10 in variance [*van Haren*, 2007], but in the present bottom boundary layer data the 10-m scales are not resolved. Unfortunately, the higher vertical scale resolution ADCP-data are too noisy to compute instantaneous shear.

[17] The computed 150-m shear is 0.7 ± 0.4N, where N is computed over much smaller, canonical 10 m intervals, hence the relatively large uncertainty bar. Note that the uncertainty in N is due to the thin-layer step-like alternation of near-homogeneous and strongly stratified layers (Figure 1b). Nevertheless, the observed values between the current meters demonstrate that the large shear is turning the water column to near marginal stability in a gradient Richardson number sense, Ri ≈ 2 ± 1.5, and the observed K-H billows occur in a period when shear is relatively large in the 18 days record (Figure 4a).

[18] Remarkably, this large shear and billow formation coincide with low contents of particles, or better acoustic scatterers, in the water: the lowest contents in a tidal period, so that the billow train is also visible in the ADCP's echo intensity as turbulent train in otherwise clear water. The relative echo intensity or backscatter strength is computed following *Gostiaux and van Haren* [2009] (Figures 4b and 4c), and resembles atmospheric radar images by *Browning and Watkins* [1970], except for a split of interface layers that is lacking in the present data.

4. Discussion

[19] The observed coupling between low-frequency tidal, high-frequency internal waves near the buoyancy frequency and super-buoyancy motions relates to an important process for diapycnal mixing. This is because the latter are associated with the largest turbulent overturns. In contrast with linear waves, they form closed contours and thus transport material. So far, the present coupling between internal wave band and turbulence scales outside it has not often been observed in the deep ocean. However, there is no reason that the GMS scenario is unique.

[20] Some details are unknown as to how the observed K-H billows are formed. This holds especially for the association of such shear-induced turbulence with local mode-2 internal waves in combination with upslope flow in the interior during the near-bottom downwelling phase of the tide/inertial motions. Of course, the tidal, or at smaller vertical scales inertial, dominance does not match with predicted time scales of processes like set-up, growth and eventual shut-down of a large boundary layer as these take longer than a day [e.g., *MacCready and Rhines*, 1993]. Our observations are also different from near-surface observations, e.g., as presented by *Marmorino* [1987], who showed trains of a few (4–5) billows, apparently in the more turbulent, final billow stage and appearing in quasi local mode-2 fashion. *Thorpe* [1987] sketched several stages of K-H roll-up and levels of turbulence. K-H stages are determined by conditions like stratification versus shear during their development. *Marmorino* [1987] suggested their generation to be due to near-inertial shear. The typical vertical length-scale of the latter is estimated at $\Delta z \approx 10$ m, accommodating estimates from microstructure observations by *Gargett et al.* [1981]. This vertical shear scale matches the vertical billow scale observed by *Marmorino* [1987] and in the present data. However, the associated much thinner interfaces of $\Delta z \approx 1$ m being folded-up by the billow are not well-resolved and *Moum et al.* [2003] suggested a sequence of overturning scales down to $\Delta z \approx 0.1$ m. Such scales are then likely driven by local small-scale internal wave shear.

[21] In the present observations the coupling is variable between near-N internal waves, either in local mode-1 or mode-2, and the apparent mode-2 structured billows. Especially the ambiguity of occurrence, during crest/trough or maximum shear, is not well-understood. Nonetheless, the coupling with the internal tidal and higher frequency waves is obvious, as are the importance of stratification and the small effects on resuspension of sediments during the warming tidal phase of clear waters. It demonstrates the importance of tidal internal wave induced mixing also above non-critical deep-ocean bottom slopes and at some distance off the bottom.

[22] **Acknowledgments.** We thank the crew of the R/V *Pelagia* for deployment and recovery of our moorings and Theo Hillebrand and NIOZ-MTM for preparation of instrumentation. We keep on enjoying discussions with Martin Laan on all aspects of NIOZ thermistor strings. Construction and deployment of "NIOZ3" were financed in part by investment grants ("Oceanographic equipment" and "LOCO", respectively) from Netherlands organisation for the advancement of scientific research, NWO and by BSIK. LG was supported in part by BSIK.

References

Abarbanel, H. D., D. D. Holm, J. E. Marsden, and T. Ratiu (1984), Richardson number criterion for the nonlinear stability of 3D stratified flow, *Phys. Rev. Lett.*, *52*, 2352–2355, doi:10.1103/PhysRevLett.52.2352.

Browning, K. A., and C. D. Watkins (1970), Observations of clear air turbulence by high power radar, *Nature*, *227*, 260–263, doi:10.1038/227260a0.

Fructus, D., M. Carr, A. Jensen, and P. A. Davies (2009), Shear-induced breaking of large internal solitary waves, *J. Fluid Mech.*, *620*, 1–29, doi:10.1017/S0022112008004898.

Gargett, A. E., P. J. Hendricks, T. B. Sanford, T. R. Osborn, and A. J. Williams III (1981), A composite spectrum of vertical shear in the upper ocean, *J. Phys. Oceanogr.*, *11*, 1258–1271, doi:10.1175/1520-0485(1981)011<1258:ACSOVS>2.0.CO;2.

Garrett, C. (1990), The role of secondary circulation in boundary mixing, *J. Geophys. Res.*, *95*, 3181–3188, doi:10.1029/JC095iC03p03181.

Gostiaux, L., and H. van Haren (2009), Extracting meaningful information from uncalibrated backscattered echo intensity data, *J. Atmos. Oceanic Technol.*, doi:10.1175/2009JTECHO704.1, in press.

Grue, J., A. Jensen, P. Rusas, and J. Sveen (2000), Breaking and broadening of internal solitary waves, *J. Fluid Mech.*, *413*, 181–218, doi:10.1017/S0022112000008648.

Haury, L. R., M. G. Briscoe, and M. H. Orr (1979), Tidally generated internal wave packets in Massachusetts Bay, *Nature*, *278*, 312–317, doi:10.1038/278312a0.

Hazel, P. (1972), Numerical studies of the stability of inviscid stratified shear flows, *J. Fluid Mech.*, *51*, 39–61, doi:10.1017/S0022112072001065.

Hosegood, P., and H. van Haren (2003), Ekman-induced turbulence over the continental slope in the Faeroe-Shetland Channel as inferred from spikes in current meter observations, *Deep Sea Res., Part I*, *50*, 657–680, doi:10.1016/S0967-0637(03)00038-4.

Hosegood, P., J. Bonnin, and H. van Haren (2004), Solibore-induced sediment resuspension in the Faeroe-Shetland Channel, *Geophys. Res. Lett.*, *31*, L09301, doi:10.1029/2004GL019544.

Howard, L. N. (1961), Note on a paper by John W. Miles, *J. Fluid Mech.*, *10*, 509–512, doi:10.1017/S0022112061000317.

Klymak, J. M., and J. N. Moum (2003), Internal solitary waves of elevation advancing on a shoaling shelf, *Geophys. Res. Lett.*, *30*(20), 2045, doi:10.1029/2003GL017706.

Ludlam, F. (1967), Characteristics of billow clouds and their relation to clear air turbulence, *Q. J. R. Meteorol. Soc.*, *93*, 419–435, doi:10.1002/qj.49709339803.

MacCready, P., and P. B. Rhines (1993), Slippery bottom boundary layers on a slope, *J. Phys. Oceanogr.*, *23*, 5–22, doi:10.1175/1520-0485(1993)023<0005:SBBLOA>2.0.CO;2.

Marmorino, G. O. (1987), Observations of small-scale mixing processes in the seasonal thermocline. Part II: Wave breaking, *J. Phys. Oceanogr.*, *17*, 1348–1355, doi:10.1175/1520-0485(1987)017<1348:OOSSMP>2.0.CO;2.

Miles, J. W. (1961), On the stability of heterogenous shear flows, *J. Fluid Mech.*, *10*, 496–508, doi:10.1017/S0022112061000305.

Mohn, C., and A. Beckmann (2002), The upper ocean circulation at Great Meteor Seamount, *Ocean Dyn.*, *52*, 179–193, doi:10.1007/s10236-002-0017-4.

Moum, J. N., D. M. Farmer, W. D. Smyth, L. Armi, and S. Vagle (2003), Structure and generation of turbulence at interfaces strained by internal solitary waves propagating shoreward over the continental shelf, *J. Phys. Oceanogr.*, *33*, 2093–2112, doi:10.1175/1520-0485(2003)033<2093:SAGOTA>2.0.CO;2.

Phillips, O. M. (1977), *Dynamics of the Upper Ocean*, 2nd ed., 336 pp., Cambridge Univ. Press, Cambridge, U. K.

Smith, W. H. F., and D. T. Sandwell (1997), Global seafloor topography from satellite altimetry and ship depth soundings, *Science*, *277*, 1957–1962.

Sveen, J. K., Y. Guo, P. A. Davies, and J. Grue (2002), On the breaking of internal solitary waves at a ridge, *J. Fluid Mech.*, *469*, 161–188, doi:10.1017/S0022112002001556.

Thorpe, S. A. (1971), Experiments on the instability and turbulence in a stratified shear flow, *J. Fluid Mech.*, *46*, 299–319, doi:10.1017/S0022112071000557.

Thorpe, S. A. (1987), Transitional phenomena and the development of turbulence in stratified fluids: A review, *J. Geophys. Res.*, *92*, 5231–5248, doi:10.1029/JC092iC05p05231.

van Haren, H. (2006), Nonlinear motions at the internal tide source, *Geophys. Res. Lett.*, *33*, L11605, doi:10.1029/2006GL025851.

van Haren, H. (2007), Shear at the critical diurnal latitude, *Geophys. Res. Lett.*, *34*, L06601, doi:10.1029/2006GL028716.

van Haren, H., M. Laan, D.-J. Buijsman, L. Gostiaux, M. G. Smit, and E. Keijzer, (2009), NIOZ3: Independent temperature sensors sampling yearlong data at a rate of 1 Hz, *IEEE J. Oceanic Eng.*, *34*, 315–322, doi:10.1109/JOE.2009.2021237.

Weatherly, G. L., and P. J. Martin (1978), On the structure and dynamics of the oceanic bottom boundary layer, *J. Phys. Oceanogr.*, *8*, 557–570, doi:10.1175/1520-0485(1978)008<0557:OTSADO>2.0.CO;2.

Woods, J. D. (1968), Wave-induced shear instability in the summer thermocline, *J. Fluid Mech.*, *32*, 791–800, doi:10.1017/S0022112068001035.

L. Gostiaux, Laboratoire des Écoulements Géophysiques et Industriels, CNRS UMR 5519, BP53, Grenoble, 38041, France.

H. van Haren, Royal Netherlands Institute for Sea Research, PO Box 59, NL-1790 AB Den Burg, the Netherlands. (hans.van.haren@nioz.nl)